

DFBVS: Deep Feature-Based Visual Servo

Nicholas Adrian, Van-Thach Do, and Quang-Cuong Pham

Abstract—Classical Visual Servoing (VS) rely on handcrafted visual features, which limit their generalizability. Recently, a number of approaches, some based on Deep Neural Networks, have been proposed to overcome this limitation by comparing directly the entire target and current camera images. However, by getting rid of the visual features altogether, those approaches require the target and current images to be essentially similar, which precludes the generalization to unknown, cluttered, scenes. Here we propose to perform VS based on visual features as in classical VS approaches but, contrary to the latter, we leverage recent breakthroughs in Deep Learning to automatically extract and match the visual features. By doing so, our approach enjoys the advantages from both worlds: (i) because our approach is based on visual features, it is able to steer the robot towards the object of interest even in presence of significant distraction in the background; (ii) because the features are automatically extracted and matched, our approach can easily and automatically generalize to unseen objects and scenes. In addition, we propose to use a render engine to synthesize the target image, which offers a further level of generalization. We demonstrate these advantages in a robotic grasping task, where the robot is able to steer, with high accuracy, towards the object to grasp, based simply on an image of the object rendered from the camera view corresponding to the desired robot grasping pose.

I. INTRODUCTION

Visual Servoing (VS), where images recorded from a camera mounted on the robot end-effector are used to iteratively guide the robot motions, is a key technique to tackle robotic tasks requiring high accuracy (see e.g. [1] for a review). Classical approaches to VS require handcrafting visual features, such as points, lines, or corners, which limit their generalizability.

Recently, a number of approaches have been proposed to overcome the reliance of classical VS on handcrafted features. In [2], [3], the authors considered the whole image as a single feature to circumvent the need to construct and extract special features. In [4]–[7], Convolutional Neural Networks (CNNs) are used on whole images, either to directly estimate the pose difference between the target and current image, or to find the instantaneous robot control in an end-to-end manner.

We argue that getting rid of the visual features altogether is akin to throwing the baby out with the bathwater. Indeed, by comparing directly the entire target and current images, the approaches just mentioned require those two images to be essentially similar, which precludes the *generalization to unknown, cluttered, scenes*. Consider for instance the situation of Fig. 1, where the object of interest is isolated in

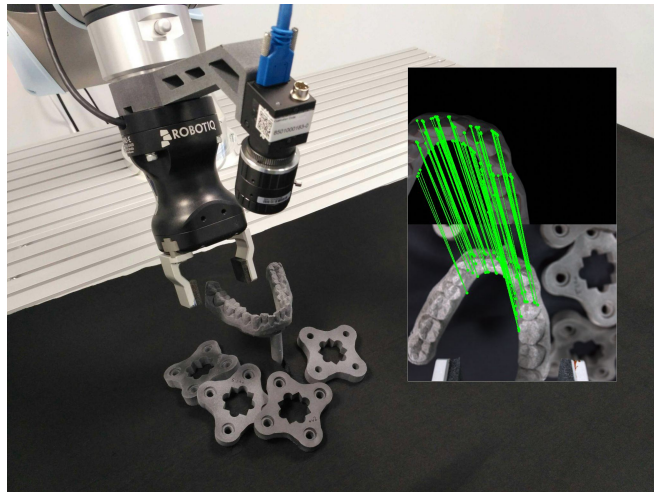


Fig. 1: Visual Servoing on a 3D printed object. A Deep Neural Network (*not* trained on the object at hand) outputs rich feature points separately on two images: target (top) and current (bottom) images, forming feature correspondences despite dissimilar backgrounds. The target image is rendered from the object’s CAD model viewed from the desired grasping pose. The video of the experiments is available at <https://youtu.be/vFAdebgog7k>.

the target image, but surrounded by distractors in the current image. Approaches based on “whole-image” processing will fundamentally be unable to steer the robot towards the target camera view of the object of interest because the two images are too different.

On the contrary, a feature-based approach will enjoy an *attention-like* mechanism: if one can match a sufficient number of features *on the object of interest* in the target and current images, Visual Servoing will be possible even in the presence of significant distraction. Building on this insight, we propose here to perform VS based on visual features as in classical VS approaches. But contrary to the latter, we leverage recent breakthroughs in Deep Learning [8]–[11] to *automatically* extract and match those visual features between the current and the target images. Our approach therefore enjoys the following advantages as compared to the literature:

- because our approach is based on visual features, it is able to steer the robot towards the object of interest even in presence of significant distraction in the background;
- because the features are automatically extracted and matched, our approach can easily and automatically generalize to unseen objects and scenes.

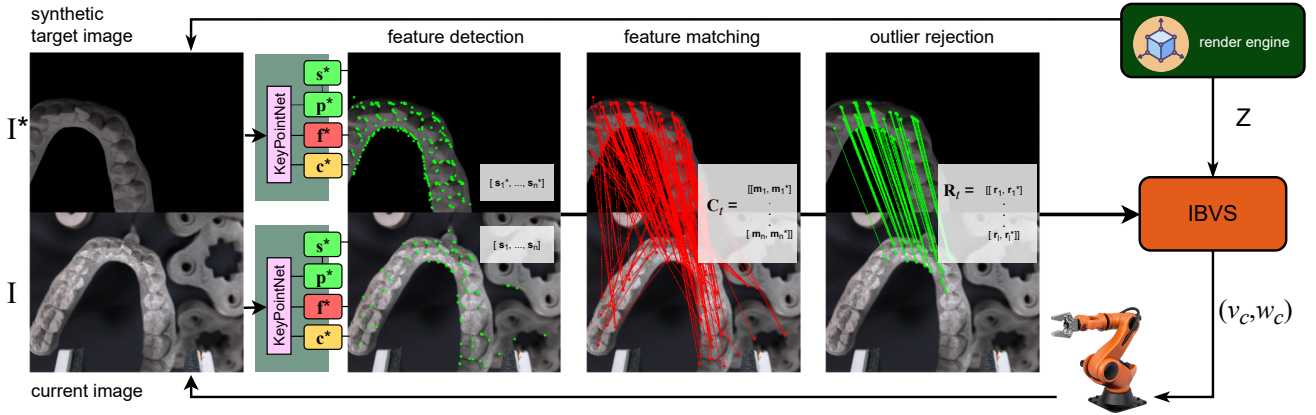


Fig. 2: Our proposed pipeline for visual servoing with DL-based sparse feature detection (Section IV-B), feature matching (Section IV-C), and outlier rejection (Section IV-C). Render engine (Section IV-A) renders the target image and provides accurate depth values as part of the required input to IBVS control law (Section III).

In addition, we propose to use a render engine to synthesize the target image. This enables a simple and automatic way to acquire the target image, while providing, moreover, accurate depth values for the visual features. Note that this “sim-to-real” idea is made possible only by the attention-like mechanism discussed previously. Figure 2 shows the flowchart of the overall pipeline.

The remainder of the paper is organized as follows. In Section II, we review related works in visual servoing, emphasizing on methods that utilize Deep Neural Network (DNN). In Section III, we present brief theoretical background behind Image-Based Visual Servo (IBVS) control which our method relies on. The components of DFBVS are elaborated in Section IV. In Section V we show that our method can achieve accurate positioning (0.89 pixels average error) and convergence on three unseen objects despite significant distraction on the current image. Finally, we conclude in Section VI.

II. LITERATURE REVIEW

A. Classical Visual Servo

In general, classical visual servoing consists of two classes: Image-Based Visual Servo (IBVS) and Position-Based Visual Servo (PBVS) [1]. In IBVS [12], [13], the features are directly obtained from the image measurement. While in PBVS [14], the image measurement is further developed into 3D parameters. Generally, PBVS is more computationally demanding due to the need to establish 2D-3D correspondence for each feature and thus requires camera intrinsic parameters and the object’s 3D model while IBVS only requires the former (this simplicity in feature calculation is the reason why we base our method on IBVS). PBVS control scheme theoretically can achieve global asymptotic stability but under the strict requirement for correct calculation of 3D parameters, else it affect the final accuracy. On the other hand, IBVS has local asymptotic stability at best but is more robust towards errors in calibration and depth estimation. In both classes, classical visual servoing methods

rely on extracting hand-crafted visual features, which is error-prone and has limited generalizability.

Direct visual servoing (DVS) [2], [3] was designed to circumvent the need for image feature extraction. Instead, analytical calculation of interaction matrix based on illumination model is used to link temporal variation of whole image luminance values with image motion. While it can achieve lower positioning error compared to classical visual servoing, it has smaller convergence domain.

B. Deep Learning (DL) for Visual Servo

DL is increasingly explored to improve existing visual servoing methods. Most approaches wager that such improvement can be obtained through dropping reliance on extracting visual features.

In [4], the network is trained to compute relative camera pose between two images. A PBVS controller is then employed to calculate the velocity command for a quadrotor. Similarly in [5], the first network iteration is trained to find relative camera pose from a single current image while the target image is implicitly learned. In their attempt to generalize, the second network iteration is modified to accept two images corresponding to two viewpoints of the same scene and outputs the relative camera pose between the images. The error is then passed to a PBVS controller for servoing. This pipeline was tested on an unseen scene and managed to achieve convergence of few centimeters.

In [6], the network outputs the relative camera pose (eye-in-hand) which can be followed as a one-shot motion or in iterative manner. The network achieved sub-millimeter positioning accuracy and was tested on a related but unseen VGA connector.

In [7], the DEFNet outputs the relative end-effector pose (eye-to-hand) and similarly achieves sub-millimeter positioning accuracy. More interestingly, the network was tested on four other unseen objects at various lighting conditions and achieved sub-millimeter positioning accuracy on most of

them. However, the position difference between the initial and target pose is limited to few millimeters.

Another approach, DFVS [15], utilizes DNN (based on FlowNet2 [16]) to output optical flow from two images while another network estimates the depth value for each feature.

All of the mentioned DL-based methods rely on direct comparison of whole images instead of extracting visual features. Thus, these approaches require the current and target images to be essentially similar which limits generalizability. Furthermore, [4]–[7], impose the heavy demand of estimating the full 6D pose on the DNN. We argue that this put further limitation on generalizability. Instead of estimating 6D pose, our network explicitly detect features on 2D image. Arguably, detecting 2D features is easier compared to estimating 6D pose.

C. Deep Learning for Feature Extraction

Feature extraction, more specifically for keypoints, have been implemented in many areas such as in calibration and localization. Traditionally, people rely on hand-crafted algorithms to detect keypoints [17]–[19]. The breakthrough in DL has allowed DNN to replace the traditional algorithms and achieves better performance and robustness against occlusion and variable lighting conditions. More recently, there has been increased attention in *self-supervised* network for keypoint detection — that is, they do not require manual human labelling. LF-Net [8] performs training with images of buildings but the training pipeline requires integration of Structure-from-Motion (SfM) algorithm. SuperPoint [9] pretrains the base detector using synthetic data of simple geometries. UnsuperPoint [10] removes the pretraining requirement and improves on the operation speed. KP2D [11] made follow-up improvement by introducing outlier rejection during training and better keypoint regression method.

D. Object Pose Estimation

Object pose estimation from an RGB image is a closely related topic. One approach relies on directly estimating the 6D pose in a single shot [20]. Another approach predicts 2D keypoints in the image before computing object pose through establishing 2D-3D correspondences [21]–[23]. These CNN-based methods have outperformed the traditional methods [17], [18] in terms of accuracy and robustness to lighting and occlusion. [24], [25] are some of the best performing methods which score highly on the LINEMOD dataset [26]. One of the evaluation metrics that they use is the 2D projection metric. With this, they measure the difference between projected object’s vertices in the 2D image between ground-truth and the estimated object pose. The estimated pose is considered correct if the average pixel difference is below 5 pixels (for 480x640 image). Another well-known metric is the 5° , $5cm$ metric where the estimated pose is considered correct if the rotation is under 5° and translation under 5 cm respectively.

III. BACKGROUND ON IBVS

Here we provide a short introduction to IBVS that is relevant to our control application. For more explanation,

we refer the reader to [1].

The goal of IBVS is to minimize the error between features obtained in the image space.

$$\mathbf{e}(t) = \mathbf{s}(\mathbf{p}(t), \boldsymbol{\xi}) - \mathbf{s}^*(\mathbf{p}^*, \boldsymbol{\xi}) \quad (1)$$

In the equation above, $\mathbf{p} = (u_1, v_1, \dots, u_k, v_k) \in \mathbb{R}^{2k}$ contains the set of 2-D pixel coordinates of k features in the current image \mathbf{I} . The pixel values are converted to the image plane cartesian coordinate $\mathbf{s} = \mathbf{s}(\mathbf{p}(t), \boldsymbol{\xi}) = (x_1, y_1, \dots, x_k, y_k) \in \mathbb{R}^{2k}$ using the set of camera intrinsic parameters $\boldsymbol{\xi}$. Similarly, \mathbf{p}^* and \mathbf{s}^* are measurements obtained from the target image \mathbf{I}^* .

The spatial velocity expressed in camera frame, or camera twist, is defined as $\mathbf{v}_c = (v_x, v_y, v_z, w_x, w_y, w_z) \in \mathbb{R}^6$ and is related to \mathbf{s} by the equation:

$$\dot{\mathbf{s}} = \mathbf{L}(\mathbf{s}, \mathbf{Z})\mathbf{v}_c \quad (2)$$

where $\mathbf{L}(\mathbf{s}, \mathbf{Z}) \in \mathbb{R}^{2k \times 6}$ is the interaction matrix, and $\mathbf{Z} \in \mathbb{R}^k$ is the feature depth vector.

From (1) and (2), we obtain:

$$\dot{\mathbf{e}} = \mathbf{L}(\mathbf{s}, \mathbf{Z})\mathbf{v}_c \quad (3)$$

To achieve an exponential decoupled decrease of error, a classical IBVS control law [1] is adopted as follows:

$$\mathbf{v}_c = -\lambda \hat{\mathbf{L}}^+(\mathbf{s}, \mathbf{Z})\mathbf{e} \quad (4)$$

where $\hat{\mathbf{L}}$ is an approximation of \mathbf{L} . There are several ways to construct $\hat{\mathbf{L}}$ [1]. In our implementation, we use $\hat{\mathbf{L}}(\mathbf{s}, \mathbf{Z}) = \mathbf{L}_*(\mathbf{s}^*, \mathbf{Z}^*)$ which is the value of \mathbf{L} at the target pose as captured in \mathbf{I}^* .

IV. DEEP FEATURE-BASED VISUAL SERVO (DFBVS)

A. Render Engine

In robotic *grasping* or *inspection* operation, typically the target end-effector or camera pose relative to the target object is specified from a motion planner. However, converting the target pose to target image for visual servoing is riddled in paradox: if one can operate the robot accurately to obtain the target image \mathbf{I}^* , there is no longer a need for visual servoing. When collaborative robot is in the picture, hand-guiding for \mathbf{I}^* becomes a feasible option albeit highly challenging when high accuracy is required.

The implementation of an image render engine allows us to circumvent said paradox quickly. We apply Eevee renderer in Blender 3D software to directly generate \mathbf{I}^* from the target pose. The render engine also simplifies the requirement for depth values of features in constructing $\hat{\mathbf{L}}$. By choosing $\hat{\mathbf{L}} = \mathbf{L}_*$, the target feature depth vector \mathbf{Z}^* can be easily obtained from the render engine.

B. Feature Extraction

The KeyPointNet network [11], $K : \mathbf{I} \rightarrow \{\mathbf{p}, \mathbf{f}, \mathbf{c}\}$, takes an input image and outputs a set of n keypoints \mathbf{p} (similar in (1)), descriptors $\mathbf{f} \in \mathbb{R}^{n \times 256}$, and normalized confidence score $\mathbf{c} \in \mathbb{R}^n$.

The network is trained in a self-supervised manner with weighted combination of loss functions. The authors claimed

TABLE I: Experiment result for robotic grasping on three objects

experiment	$ \Delta x, \Delta y, \Delta z $ [mm]	$ \Delta r_x, \Delta r_y, \Delta r_z $ [deg]	AVG1 [px]	AVG2 [px]
O ₁ G ₁ T ₁	3.25, 3.49, 67.72	10.42, 6.70, 0.13	0.71	0.78
O ₁ G ₁ T ₂	2.88, 0.13, 86.04	15.01, 3.78, 0.17	1.14	1.19
O ₁ G ₁ T ₃	21.22, 11.45, 64.94	7.61, 9.39, 7.87	1.00	1.28
O ₁ G ₂ T ₁	13.86, 16.90, 49.17	4.27, 6.28, 4.74	0.89	1.07
O ₁ G ₂ T ₂	3.12, 12.25, 51.63	6.78, 3.66, 1.05	0.74	1.12
O ₁ G ₂ T ₃	3.81, 14.94, 57.53	6.86, 4.61, 1.31	1.04	1.39
O ₂ G ₁ T ₁	1.00, 12.36, 59.18	7.67, 2.99, 0.74	0.85	1.13
O ₂ G ₁ T ₂	1.53, 24.47, 44.40	4.21, 1.57, 1.21	0.74	0.56
O ₂ G ₁ T ₃	1.15, 10.33, 24.12	2.85, 0.40, 0.86	0.73	0.49
O ₂ G ₂ T ₁	0.18, 11.08, 41.28	5.07, 1.98, 0.42	0.62	0.46
O ₂ G ₂ T ₂	1.49, 27.51, 43.66	3.77, 1.90, 0.96	0.65	0.59
O ₂ G ₂ T ₃	5.90, 11.79, 51.78	5.97, 3.70, 1.62	0.81	0.59
O ₃ G ₁ T ₁	27.85, 4.72, 51.49	10.88, 5.29, 1.76	1.10	0.94
O ₃ G ₁ T ₂	0.58, 12.18, 47.08	8.56, 0.12, 2.97	0.68	0.74
O ₃ G ₁ T ₃	15.51, 9.30, 56.42	9.48, 4.73, 5.41	0.63	0.94
O ₃ G ₂ T ₁	2.64, 20.5, 34.79	4.93, 0.67, 3.34	0.86	0.89
O ₃ G ₂ T ₂	8.61, 23.25, 49.68	5.15, 7.13, 1.84	1.03	1.16
O ₃ G ₂ T ₃	1.30, 20.28, 49.38	7.58, 1.83, 2.44	0.83	0.74

that this allowed them to enforce keypoint detection at different views, minimize distance between descriptors of the same feature seen at different views, maximize distance between different features and enforce consistent score from different views. We refer to the original paper for more details.

C. Feature Matching and Outlier Rejection

At each control cycle t , the features $\mathbf{s}(t)$ and \mathbf{s}^* are matched based on the descriptor values to form n correspondences \mathbf{C}_t via *nearest-neighbour* function N :

$$N : \{\mathbf{s}(t), \mathbf{f}(t), \mathbf{s}^*, \mathbf{f}^*\} \rightarrow \mathbf{C}_t \quad (5)$$

$$\mathbf{C}_t = [\mathbf{m}, \mathbf{m}^*] \in \mathbb{R}^{n \times 4} \quad (6)$$

where \mathbf{m} and \mathbf{m}^* are simply $\mathbf{s}(t)$ and \mathbf{s}^* respectively which are rearranged to form feature pairs which are close in the descriptor space.

Since $\mathbf{s}(t)$ and \mathbf{s}^* are obtained from different images, they do not necessarily have a one-to-one match (e.g. a feature in $\mathbf{I}(t)$ might not be visible in \mathbf{I}^*). Therefore, the correspondence matching in (5) is bound to produce some false correspondences. Refer to Figure 3 for an illustration.

In order to mitigate this, we implement RANSAC [27] ($R : \mathbf{C}_t \rightarrow \mathbf{R}_t, \mathbf{R}_t \subseteq \mathbf{C}_t$) on the correspondences to estimate inlier subset \mathbf{R}_t that will be used as input to the control law.

$$\mathbf{R}_t = [\mathbf{r}, \mathbf{r}^*] \in \mathbb{R}^{l \times 4} \quad (7)$$

where $\mathbf{r} \subseteq \mathbf{m}$, $\mathbf{r}^* \subseteq \mathbf{m}^*$, and $l \leq n$.

D. Establishing Tracking Behavior

At each cycle, the set of 3D points that forms the correspondences might not be identical with the set in the previous or following cycle. When this happens, we say that the system displays *correspondence-switching* behavior. Refer to Figure 4 for an illustration.

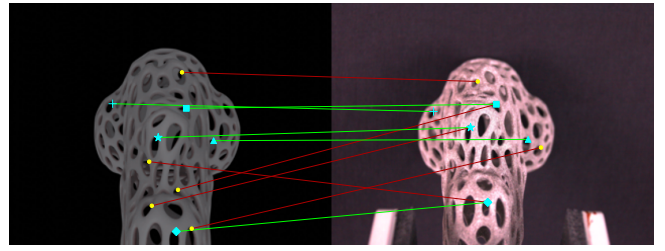


Fig. 3: Blue points indicate 3D points which are detected in both target and current images. Each pair of unique 3D point is distinguished by similar marker shape in both images. Points in yellow indicate 3D points which are not detected in the other image i.e. has no true correspondence. Performing correspondence matching will result in true correspondences shown in green and false correspondences shown in red.

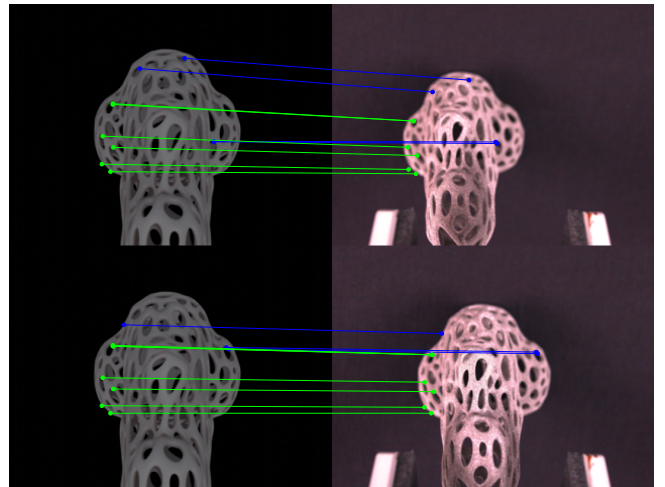


Fig. 4: (First row) Correspondences at cycle $t - 1$. (Second row) Correspondences at cycle t . (Correspondence-switch) Only the correspondences in green consistently appear in both cycles. The correspondences in blue have undergone *correspondence-switching*.

This becomes a problem when the camera pose is close to the target pose as the *correspondence-switching* causes oscillations that complicates convergence. In order to mitigate this, we enforce *tracking* behavior when the camera image is close to \mathbf{I}^* (we estimate this by taking the average of $\mathbf{e}(t)$). We notate cycles with *tracking* behavior as t' .

At t' , the correspondences are always a subset of the previous correspondences ($\mathbf{R}_{t'} \subseteq \mathbf{R}_{t'-1}$). This is obtained by matching features from current image ($\mathbf{s}(t')$) with target features which are present in previous cycle (\mathbf{r}^* at $t' - 1$) to obtain the correspondence set $\mathbf{C}_{t'}$ and the inlier set $\mathbf{R}_{t'}$ respectively.

V. EXPERIMENT

We run several experiments to assess the performance of DFBVS. The setup consists of a FLIR BFS-U3-120S4C camera with 12 mm lens installed on the end-effector of a Universal Robot UR5e manipulator.

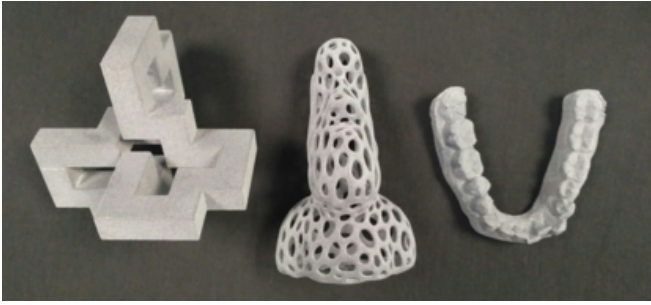


Fig. 5: Three objects O_1 , O_2 , and O_3 which were 3D printed using HP MJF5200.

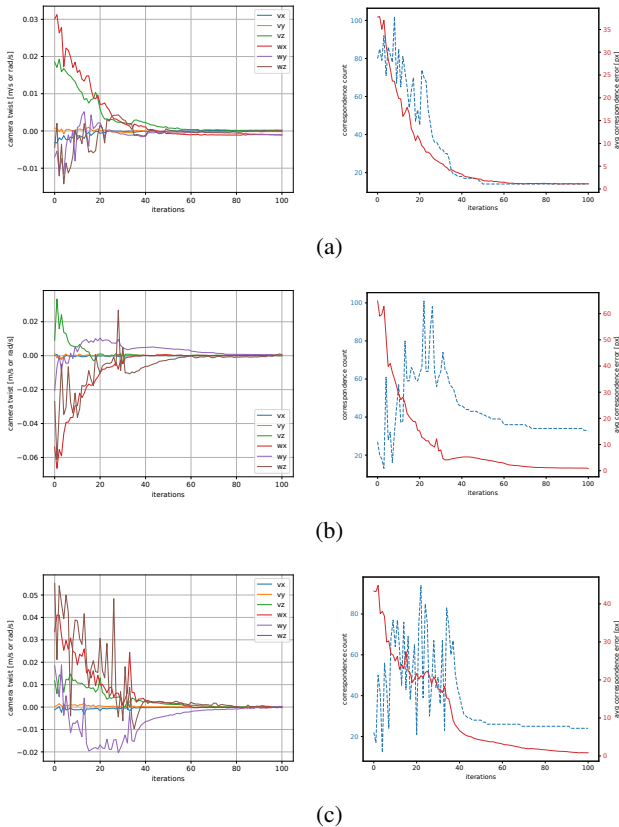


Fig. 6: Each row shows profiles from visual servoing on different unseen objects: (a) O_1 (b) O_2 (c) O_3 . Figures on the left are camera twist profiles. Figures on the right show average correspondence error in red and correspondence count in blue.

Image from the camera is downsized to 320x240 before being forwarded through the network. We chose the top 500 keypoints from the network output ranked by the confidence score c . To showcase the generalizability of the pipeline, we apply the same network weight (v4), which was trained on COCO dataset [28] by the original paper’s authors [11], without any fine-tuning. Experiments are done on unseen 3D printed objects (O_1, O_2, O_3) as seen in Figure 5. The control section is implemented with ViSP library [29].

A. Accuracy Assessment

In this section, we perform experiments to quantify the accuracy of the visual servoing pipeline. As the target image was obtained through a renderer, there is no ground-truth data available on the target robot configuration. Here, we use accuracy in the image space as the accuracy metric as inspired from pose estimation field [24], [25].

Two goal poses (G_1, G_2) expressed in the object frame are identified for each object. We visit each goal pose from three initial poses (T_1, T_2, T_3). In total there are 18 ($3 \times 2 \times 3$) unique servoing arrangements for the three objects. The absolute positional distance for servoing averaged 55.1 ± 12.2 mm and 8.7 ± 3.4 deg for orientation.

We list the experiment results in Table I. For each experiment, we present two measurements of the average final correspondences error in pixel units. The first one (AVG1) is the average error calculated from all the correspondences in the final set \mathbf{R}_{final} . For the second measurement (AVG2) we carefully select three correspondences from \mathbf{R}_{final} and report the average error. The three correspondences are selected based on the following criteria:

- every correspondence pair is visually examined to point to the same 3D point
- the three correspondences to be adequately distanced from one another

Looking at AVG2, the average error is 0.89 pixels which is lower than the threshold commonly used in pose estimation field (5 pixels) to categorize successful estimation (as mentioned in Section II-D).

In Figure 6 we show example visual servoing profiles for each object to show the system’s ability to converge. The convergence can be attributed to the *tracking* strategy (indicated by later iterations with non-increasing correspondence count).

B. Integration in a Grasping Pipeline

For the second experiment, we assess our pipeline’s effectiveness for robotic grasping. The experiment mimics a typical grasping operation in a 3D print factory. Freshly printed objects would have to be grasped from a particular pose in the environment, which is likely cluttered.

The experiments are divided into six batches where the distance that the camera has to travel increases linearly from within 1 to 6 cm, beyond which the camera image gets too blurry. The rotations along X,Y,Z axes are varied within the range $[8^\circ, 6^\circ, 3^\circ]$, $[6^\circ, 6^\circ, 4^\circ]$, and $[8^\circ, 10^\circ, 8^\circ]$ for O_1 , O_2 , O_3 respectively. Eight experiments are performed at each stage. A run is considered successful if the average correspondences error falls below 2 pixels. The background in the actual setup is kept to a simple dark background and no elaborate *tuning* was done to adjust the rendered lighting. The sharpness of the camera image is also not enforced throughout the runs. Note that there are still notable discrepancies between the two input images such as appearance of the gripper fingertips in the camera image.

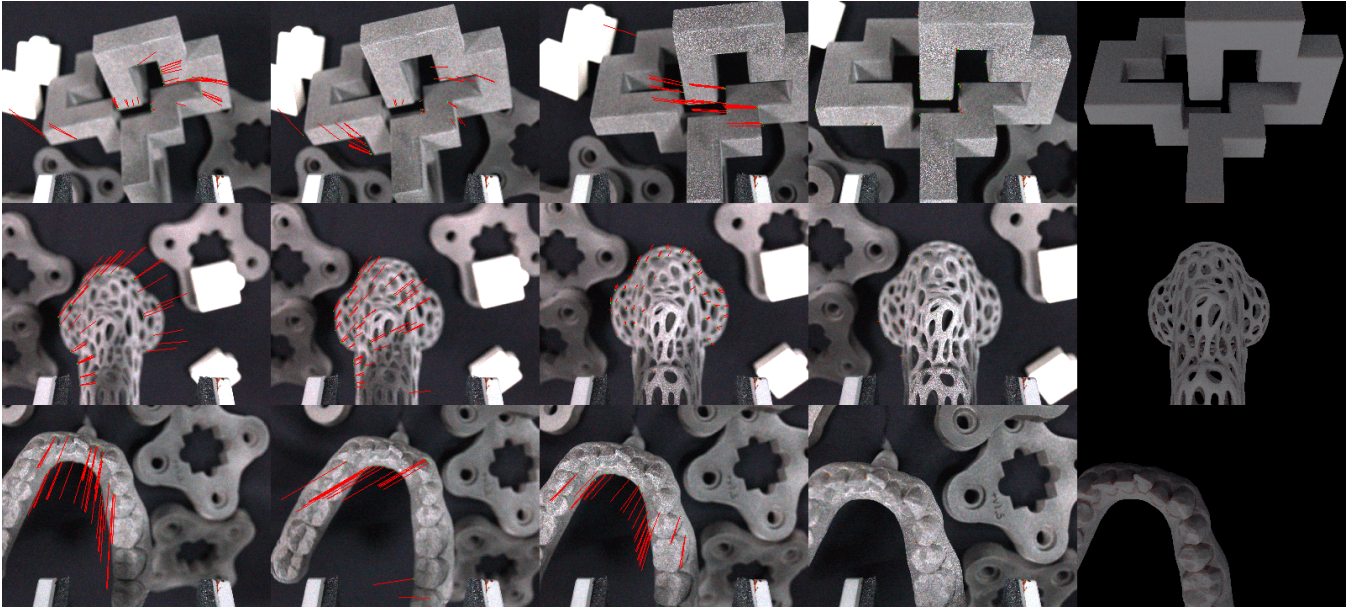


Fig. 7: Sequence of camera images from visual servoing experiments on cluttered environment with DFBVS. The feature errors, which are used as input to the IBVS control law, are displayed as red lines. The final camera images are shown on the fourth column, showing alignment with the rendered target images on the fifth column. Row 1, 2, and 3 are of object O_1 , O_2 , and O_3 respectively. Video of the experiments is available at <https://youtu.be/vFAdebgog7k>.

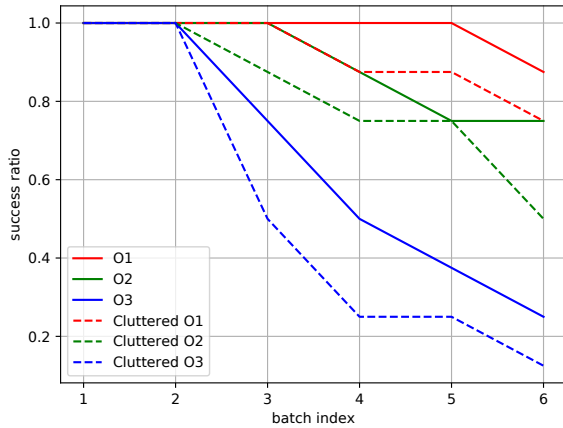


Fig. 8: Plot of grasping success ratio at each of the six batches where the distance the camera has to follow increases linearly from within 1 to 6 cm. Results for object O_1, O_2, O_3 are in red, green, and blue respectively. Experiments with similar backgrounds are in bold lines. Experiments with more challenging dissimilar backgrounds are in dashed lines. Our method achieved 100% convergence on all cases for batch 1 and 2 (within 2 cm distance).

In addition to the above, we run another set of experiments with similar setup except now we clutter the real environment with other objects. Meanwhile, the background of the rendered images remain empty.

Both results are presented in Figure 8. Results for first

experiment set are shown in bold lines while results for the second set are shown in dashed lines. Note that in all cases, the method can achieve perfect convergence when the distance between initial and final pose is within 2 cm, which can be achieved through rough positioning. Example images from the second set of experiment are displayed in Figure 7.

VI. CONCLUSION

Most recent approaches in visual servoing remove reliance on visual features and instead compare directly the target and current camera images. However, we argue that this comes at a cost of generalizability. Our proposed approach perform VS based on visual features as in classical VS approaches but, contrary to the latter, we leverage recent breakthroughs in Deep Learning to automatically extract and match the visual features. This allows our method to be generalizable to unknown, cluttered, scenes. Such generalizability furthermore allows our method to integrate a render engine to generate synthetic target image. This enables a simple and automatic way to acquire the target image, while providing accurate depth values for the visual features. For future works, we will look into applying the pipeline for assembly tasks and improving the control performance.

ACKNOWLEDGMENT

This study is supported under the RIE2020 Industry Alignment Fund – Industry Collaboration Projects (IAF-ICP) Funding Initiative, as well as cash and in-kind contribution from the industry partner, HP Inc., through the HP-NTU Digital Manufacturing Corporate Lab.

REFERENCES

- [1] F. Chaumette and S. Hutchinson, "Visual servo control. i. basic approaches," *IEEE Robotics & Automation Magazine*, vol. 13, no. 4, pp. 82–90, 2006.
- [2] C. Collewet, E. Marchand, and F. Chaumette, "Visual servoing set free from image processing," in *2008 IEEE International Conference on Robotics and Automation*, pp. 81–86, IEEE, 2008.
- [3] C. Collewet and E. Marchand, "Photometric visual servoing," *IEEE Transactions on Robotics*, vol. 27, no. 4, pp. 828–834, 2011.
- [4] A. Saxena, H. Pandya, G. Kumar, A. Gaud, and K. M. Krishna, "Exploring convolutional networks for end-to-end visual servoing," in *2017 IEEE International Conference on Robotics and Automation (ICRA)*, pp. 3817–3823, IEEE, 2017.
- [5] Q. Bateau, E. Marchand, J. Leitner, F. Chaumette, and P. Corke, "Training deep neural networks for visual servoing," in *2018 IEEE international conference on robotics and automation (ICRA)*, pp. 3307–3314, IEEE, 2018.
- [6] C. Yu, Z. Cai, H. Pham, and Q.-C. Pham, "Siamese convolutional neural network for sub-millimeter-accurate camera pose estimation and visual servoing," in *2019 IEEE/RSJ International Conference on Intelligent Robots and Systems (IROS)*, pp. 935–941, IEEE, 2019.
- [7] F. Tokuda, S. Arai, and K. Kosuge, "Convolutional neural network-based visual servoing for eye-to-hand manipulator," *IEEE Access*, vol. 9, pp. 91820–91835, 2021.
- [8] Y. Ono, E. Trulls, P. Fua, and K. M. Yi, "Lf-net: Learning local features from images," *arXiv preprint arXiv:1805.09662*, 2018.
- [9] D. DeTone, T. Malisiewicz, and A. Rabinovich, "Superpoint: Self-supervised interest point detection and description," in *Proceedings of the IEEE conference on computer vision and pattern recognition workshops*, pp. 224–236, 2018.
- [10] P. H. Christiansen, M. F. Kragh, Y. Brodskiy, and H. Karstoft, "Unsuperpoint: End-to-end unsupervised interest point detector and descriptor," *arXiv preprint arXiv:1907.04011*, 2019.
- [11] J. Tang, H. Kim, V. Guizilini, S. Pillai, and R. Ambrus, "Neural outlier rejection for self-supervised keypoint learning," in *International Conference on Learning Representations*, 2020.
- [12] J. T. Feddema and O. R. Mitchell, "Vision-guided servoing with feature-based trajectory generation (for robots)," *IEEE Transactions on Robotics and Automation*, vol. 5, no. 5, pp. 691–700, 1989.
- [13] L. Weiss, A. Sanderson, and C. Neuman, "Dynamic sensor-based control of robots with visual feedback," *IEEE Journal on Robotics and Automation*, vol. 3, no. 5, pp. 404–417, 1987.
- [14] W. J. Wilson, C. W. Hulls, and G. S. Bell, "Relative end-effector control using cartesian position based visual servoing," *IEEE Transactions on Robotics and Automation*, vol. 12, no. 5, pp. 684–696, 1996.
- [15] Y. Harish, H. Pandya, A. Gaud, S. Terupally, S. Shankar, and K. M. Krishna, "Dfvs: Deep flow guided scene agnostic image based visual servoing," in *2020 IEEE International Conference on Robotics and Automation (ICRA)*, pp. 9000–9006, IEEE, 2020.
- [16] E. Ilg, N. Mayer, T. Saikia, M. Keuper, A. Dosovitskiy, and T. Brox, "FlowNet 2.0: Evolution of optical flow estimation with deep networks," in *Proceedings of the IEEE conference on computer vision and pattern recognition*, pp. 2462–2470, 2017.
- [17] D. G. Lowe, "Object recognition from local scale-invariant features," in *Proceedings of the seventh IEEE international conference on computer vision*, vol. 2, pp. 1150–1157, Ieee, 1999.
- [18] H. Bay, A. Ess, T. Tuytelaars, and L. Van Gool, "Speeded-up robust features (surf)," *Computer vision and image understanding*, vol. 110, no. 3, pp. 346–359, 2008.
- [19] E. Rublee, V. Rabaud, K. Konolige, and G. Bradski, "Orb: An efficient alternative to sift or surf," in *2011 International conference on computer vision*, pp. 2564–2571, Ieee, 2011.
- [20] Y. Xiang, T. Schmidt, V. Narayanan, and D. Fox, "Posecnn: A convolutional neural network for 6d object pose estimation in cluttered scenes," 2018.
- [21] M. Rad and V. Lepetit, "Bb8: A scalable, accurate, robust to partial occlusion method for predicting the 3d poses of challenging objects without using depth," in *Proceedings of the IEEE International Conference on Computer Vision*, pp. 3828–3836, 2017.
- [22] B. Tekin, S. N. Sinha, and P. Fua, "Real-time seamless single shot 6d object pose prediction," in *Proceedings of the IEEE Conference on Computer Vision and Pattern Recognition*, pp. 292–301, 2018.
- [23] M. Oberweger, M. Rad, and V. Lepetit, "Making deep heatmaps robust to partial occlusions for 3d object pose estimation," in *Proceedings of the European Conference on Computer Vision (ECCV)*, pp. 119–134, 2018.
- [24] Y. Li, G. Wang, X. Ji, Y. Xiang, and D. Fox, "Deepim: Deep iterative matching for 6d pose estimation," in *Proceedings of the European Conference on Computer Vision (ECCV)*, pp. 683–698, 2018.
- [25] S. Peng, Y. Liu, Q. Huang, X. Zhou, and H. Bao, "Pvnet: Pixel-wise voting network for 6dof pose estimation," in *Proceedings of the IEEE/CVF Conference on Computer Vision and Pattern Recognition*, pp. 4561–4570, 2019.
- [26] S. Hinterstoisser, V. Lepetit, S. Ilic, S. Holzer, G. Bradski, K. Konolige, and N. Navab, "Model based training, detection and pose estimation of texture-less 3d objects in heavily cluttered scenes," in *Asian conference on computer vision*, pp. 548–562, Springer, 2012.
- [27] M. A. Fischler and R. C. Bolles, "Random sample consensus: a paradigm for model fitting with applications to image analysis and automated cartography," *Communications of the ACM*, vol. 24, no. 6, pp. 381–395, 1981.
- [28] T.-Y. Lin, M. Maire, S. Belongie, J. Hays, P. Perona, D. Ramanan, P. Dollár, and C. L. Zitnick, "Microsoft coco: Common objects in context," in *European conference on computer vision*, pp. 740–755, Springer, 2014.
- [29] E. Marchand, F. Spindler, and F. Chaumette, "Visp for visual servoing: a generic software platform with a wide class of robot control skills," *IEEE Robotics and Automation Magazine*, vol. 12, pp. 40–52, December 2005.